



## Transition failure stress in a chain of brittle elastic beads under impact



Dongxin Liu, Luming Shen <sup>\*</sup>, Francois Guillard, Itai Einav

School of Civil Engineering, The University of Sydney, NSW 2006, Australia

### ARTICLE INFO

#### Article history:

Received 3 October 2015

Received in revised form 18 January 2016

Accepted 6 March 2016

Available online 10 March 2016

#### Keywords:

Brittle grains

Material point method

Stress propagation

Impact

Failure

### ABSTRACT

High strain rate experiments of chains of glass beads under impact loading demonstrate that first failure develops in either the first or second glass bead, depending on the impact velocity and associated stress propagation. Motivated by this notion of 'transition failure stress' we present a series of three-dimensional dynamic simulations of a 10 brittle elastic beads chain under impact of a stiffer elastic bar using the material point method (MPM). The numerical simulation results show that, as observed in the experiments, failure would first form in either the first or second closest brittle elastic bead to the impacting bar, depending on the parametric ratio between an impact-induced maximum tensile stress to fracture strength. Further non-dimensional analysis by varying materials and system parameters in the simulations suggests that this transition failure stress exists universally in brittle materials under impact loading.

© 2016 Elsevier Ltd. All rights reserved.

### 1. Introduction

Stress waves in granular materials have received extensive attention [1–6]. In brittle granular materials, stress waves can create further implications related to fabric collapse and grain crushing [7–9]. They are pivotal in geoscience, for example in studying earthquakes fault gouges and meteoritic impacts [10,11], and in many industries, including addressing mining and mineral processes, petroleum production, and in pharmaceuticals [12–14]. A key challenge is that the propagation of stress waves is controlled by the discrete nature of these materials and the dynamic behaviour of the individual grains. Most studies have dealt with stress waves where permanent irreversible effects such as damage and failure of the material may be disregarded [1]. However, in brittle granular materials the effect of permanent deformations on the propagation of stress waves should be considered [7,8]. Grain crushing may occur after the passing of strong stress waves, with fragments 'rattling' in the free voids [15]; this enhances alterations of porosity, stiffness, and permeability, all being crucial properties for predicting hydromechanical response of geo-environmental modifications. For example, Valdes et al. [16] revealed new forms of fragmentation waves in systems with intrinsically porous brittle grains, in the form of compaction bands propagating either periodically or intermittently. This distinction in the modes of propagation has recently been explained by Guillard et al. [17] through a new heuristic lattice spring

model along with newly discovered dynamic compaction patterns in brittle porous media.

Due to the effects of the interactions among contacting grains under impact loading and the resulting damage, fracture and fragmentation of the individual grains, the propagation of stress wave in multi-grain system can be very complicated. Hence, studying the response of a chain of brittle spheres under impact loading can be a simple and effective way to begin tackling this complicated problem. Job et al. [18] conducted research on the law of solitary wave propagating in the linear chain of beads using experiments and numerical simulations. They proved that the characteristics of solitary waves could be influenced by the mechanical properties of the reflection boundary. Pal et al. [19] investigated the effects of plasticity in wave propagation in a chain of elasto-plastic granular system using the finite element method. The simulations revealed that energy dissipation could lead to the formation and merging of wave trains, which have characteristics that are very different from those of elastic chains. More recently, Wang and Nesterenko [20] studied, experimentally and numerically, the attenuation of short and strongly nonlinear stress waves in dissipative chains of alternatively arranged cylinders and spheres. They demonstrated that pulses in systems with a smaller cylinder to sphere mass ratios attenuate faster.

Motivated by the abovementioned problems, this paper explores the following question: in a chain of brittle beads, which bead is likely to fail first under an impact-induced stress wave? This question has been motivated by our recent impact tests on chains of glass beads. Specifically, these tests show that it is often the second closest bead to an impacting bar that fractures first among all the loaded beads. The question here is whether this phenomenon merely

<sup>\*</sup> Corresponding author. School of Civil Engineering, The University of Sydney, NSW 2006, Australia. Tel.: +61 2 93512126; Fax: +61 2 93513343.

E-mail address: [luming.shen@sydney.edu.au](mailto:luming.shen@sydney.edu.au) (L. Shen).

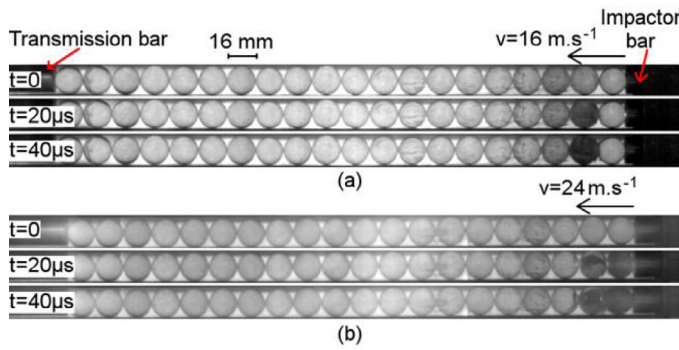


**Fig. 1.** Side view of the experimental impact tests of chains of glass beads in split Hopkinson bar device, using high-speed camera at 50,000 fps, for impact velocity of (a) 16 m/s and (b) 24 m/s. Darkening of a bead indicates complete splintering.

depends on material heterogeneities, or whether it may also be dictated by parameters such as impact velocity, duration of pulse or friction between granular particles, etc.

To better understand our previous experiments, we perform three-dimensional material point method (MPM) simulations to investigate the behaviour of a chain of 10 brittle elastic beads under the impact of a stiffer bar. Following the setup of the experiments, in the first numerical simulations, the mechanical properties of steel have been assigned to the bars ( $E_s = 210$  GPa,  $\rho_s = 7800$  kg/m<sup>3</sup>), while those of glass have been assigned to the beads ( $E_g = 70$  GPa,  $\rho_g = 2500$  kg/m<sup>3</sup>). The MPM is an extension of the particle-in-cell (PIC) method in computational fluid dynamics [21] to computational solid dynamics [22–24]. The motivation of the development was to study those problems with history-dependent internal state variables, such as contact/impact, penetration/perforation and fragmentation without invoking master/slave nodes and global remeshing. The MPM takes advantages of both Eulerian and Lagrangian methods. The mesh distortion problem in Lagrangian method can also be avoided through mapping to a mesh that can be controlled by the user [25]. Moreover, the MPM enables to naturally identify contacts between grains and to address the mesh distortion issues common in mesh-based methods due to the large deformation of particles [26].

The purpose of this study is to understand how stress wave propagation may induce damage in chains of brittle elastic grains under impact and to investigate if the friction coefficient, the initial impact velocity and the length of the impacting bar will affect the failure patterns in the chain using the 3D MPM simulations. More importantly, we aim to explain how the position of the first failure of a bead in the chain is influenced by the abovementioned factors as a function of the material strength and impact velocity.

## 2. Methods and procedures

### 2.1. Impact experiments

The numerical study performed has been motivated by experimental observations of the breaking of glass beads in a split

**Table 1**  
Different simulation parameters.

Impact velocity (m/s)		Length of impacting bar (mm)			Friction coefficient		
2.5		200			0.4		
1.5	5 10	200			0.4		
2.5		100	300	400	0.4		
2.5		200			0	0.2	0.6

Hopkinson bar device. In these experiments, a horizontal row of 20 glass beads kept in a channel are impacted at high velocity by a steel bar. The side view of the row of beads is recorded using a high-speed camera at 50,000 fps and the beads undertaking fracture get darker due to the increased diffusion of light where the glass is damaged. Fig. 1a shows that at low impact velocity, the second closest bead to the impacting bar is being severely damaged first, whereas the first closest remains almost intact. When increasing the impact velocity (Fig. 1b), we observe concurrent severe failure in the first and second closest beads to the impacting bar. These experiments suggest that there may be a transition between the low velocity case, where the first bead remains intact or slightly damaged, to a higher velocity case, where it completely breaks. Repetitions of these experiments provide similar outcomes, and therefore the reason for this phenomenon must mostly be related to deterministic material properties. The focus of this paper is therefore to explore this transition computationally by varying deterministically both system and model parameters.

### 2.2. Numerical simulation

To understand the transition in the breaking behaviour of a chain of glass beads upon impact, we perform numerical simulations using the MPM available in Uintah software [27]. The proposed problems and the simulation results are visualised using VisIt [28]. Fig. 2 shows the simulated problem where a stiff elastic bar impacts a chain of brittle elastic beads of diameter  $D = 14$  mm form a horizontal chain contacting the left bar with 14 mm diameter and 200 mm length as a base. On the right end of the beads chain, another stiff elastic bar that shares the same length and diameter as the left bar impacts on the first elastic bead. In the simulation, the elastic bars and beads are axially aligned. The initial velocity of the impacting bar is 2.5 m/s. The friction coefficient of the beads in this reference simulation is 0.4.

In order to find whether the initial impact velocity, the length of impacting bar and the friction coefficient will affect the dynamic responses of the brittle elastic beads to impact loading, different simulations are carried out, as shown in Table 1. The first row of Table 1 illustrates the initial conditions of the reference simulation. In the other simulations listed in the second to fourth rows, the impact velocity, the length of impacting bar and the friction coefficient respectively are varied while keeping the other parameters fixed. However, we observe that the dynamics is only slightly affected by the friction coefficient. Indeed, this is confirmed when using different friction coefficients, as outlined in the fourth row of Table 1 while keeping the other parameters the same as those in the

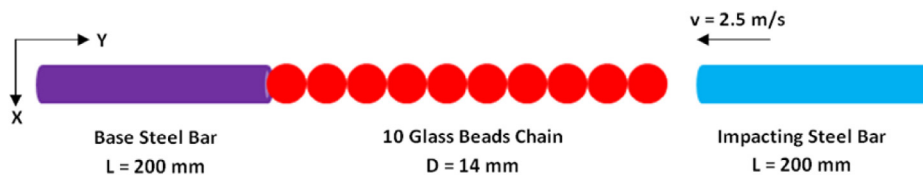


**Fig. 2.** Schematic of the simulated impact problem.

reference simulation. This is mainly because the centres of the beads are aligned along one straight line so that the limited relative frictional motion has very small influence on the magnitude of the shear stresses. In all the following simulations, we keep the friction coefficient equal to 0.4.

### 2.3. Mesh convergence study

Similar to other numerical methods, the results of the MPM can be mesh size dependent [24,26,27]. A mesh convergence study is thus performed first to find the mesh size that leads to efficient simulations with accurate results. In the mesh convergence study, a bar with elastic properties of steel ( $E_s = 210$  GPa,  $\rho_s = 7800$  kg/m<sup>3</sup>) impacting a cylinder with elastic parameters of glass ( $E_g = 70$  GPa,  $\rho_g = 2500$  kg/m<sup>3</sup>) is simulated as shown in Fig. 3a. The cylinder instead of sphere target is chosen because the analytical solution is known for this particular impact problem.

In this process, the cylindrical specimen is 140 mm long (same length as that of the 10 brittle elastic beads chain problem) with diameter of 14 mm. Other dimensions are kept the same with the initial velocity of the impacting bar still being 2.5 m/s. In these test simulations, cubic cells are used with four different mesh sizes, namely 1.4 mm, 0.7 mm, 0.35 mm and 0.175 mm. There are two material points along each direction with a total of 8 material points in each 3D cell. Fig. 3b shows the stress history in the impact direction ( $\sigma_y$ ) of a selected point A on the central axis of the cylinder, as shown in Fig. 3a, with different mesh sizes. In this figure, the simulation time  $t$  is normalised by the duration time that stress wave propagates to the other end of the specimen and reflects back to the impact surface:  $t_d = 2L_g/c_g = 54 \mu\text{s}$ , where  $L_g$  is the length of the cylinder and  $c_g$  is the wave speed in the specimen.

The analytical solution of stress history at point A is also shown in Fig. 3b. The simulated stress histories of point A are similar to the analytical solution for mesh sizes of 0.175 mm, 0.35 mm and 0.7 mm,

with the most refined mesh giving results closest to the analytical solution, but needing a larger computation time. When the mesh size is 1.4 mm, however, the stress history at the chosen points is apparently different from the other three cases as well as the analytical solution. As a result, a mesh size of 0.35 mm is adopted in this study.

## 3. Results and discussion

### 3.1. Reference simulation

To allow easy comparison, a reference simulation is defined with simulation parameters listed in the first row of Table 1. A simple model of brittle elastic material is that it will fail when the maximum principal stress  $\sigma_1$  exceeds the tensile strength of the material. In order to find the failure location in the brittle elastic beads, we plot in Fig. 4 the material points in colours if the maximum principal stress  $\sigma_1$  of that material point is higher than the tensile strength of glass, i.e.,  $R_g = 33$  MPa. The rest of the points take a grey colour. Here,  $\sigma_{max}$  represents the largest value of  $\sigma_1$  of all points in the beads chain, while  $t$  is the simulation time when the snapshot is taken. In this figure, the point is plotted in pink if its maximum principal stress exceeds 300 MPa.

Fig. 4a–c shows the distribution of the maximum principal stress in the beads chain at time of 12  $\mu\text{s}$ , 178  $\mu\text{s}$  and 250  $\mu\text{s}$  after the impact, respectively. From Fig. 4a, it is clear to see that at time  $t = 12 \mu\text{s}$ , some material points on the right of the second bead are above  $R_g$ , suggesting that these could be the first failure points in the chain under impact. These failure points first appear on the right surface of the second sphere and then at the same area in the following spheres. Eventually, a critical failure circle is formed from the second bead to the seventh bead in similar locations. In the beginning, the maximum principal stress of the first bead is less than 33 MPa under the given impact velocity, which means that generally no failure is expected to occur in the first sphere under the current loading conditions.

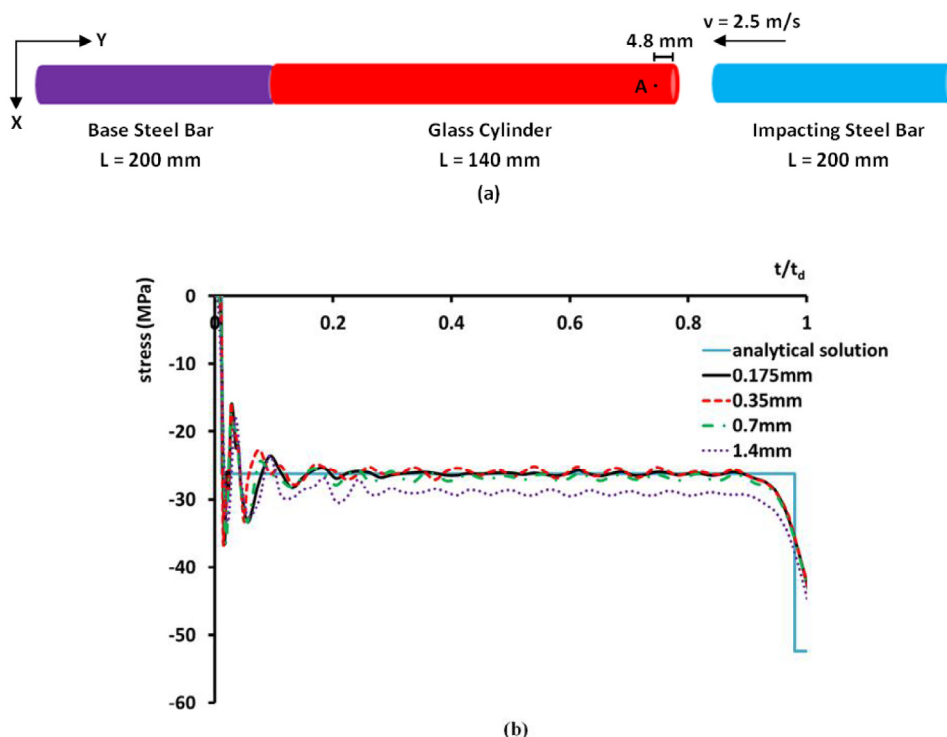


Fig. 3. (a) Schematic of the mesh convergence study problem. (b) History of stress in the impact direction ( $\sigma_y$ ) at point A with different mesh sizes.

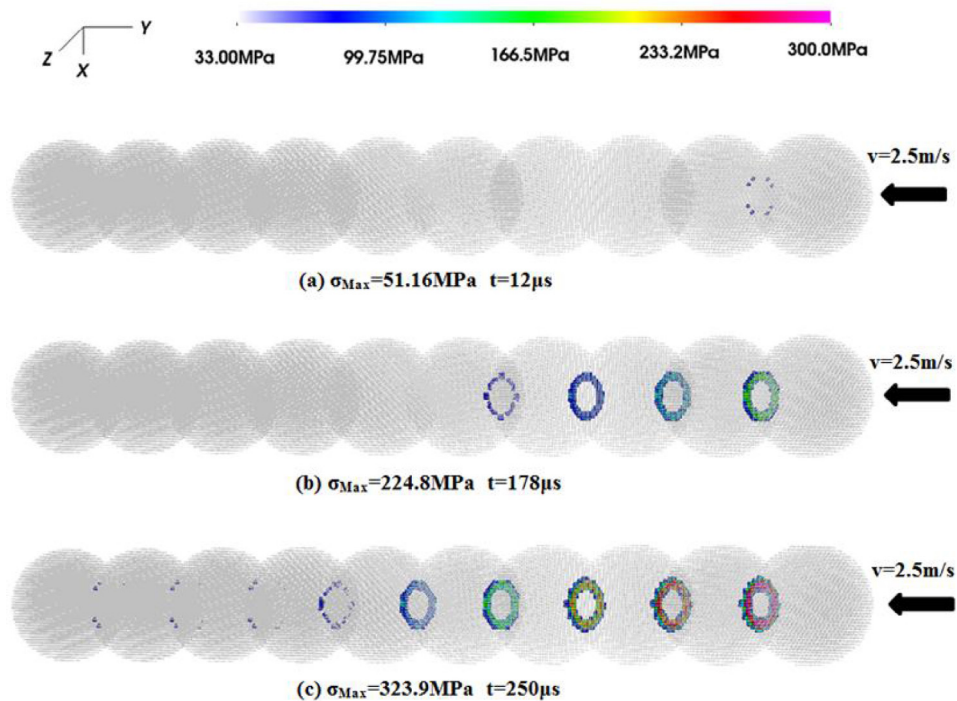


Fig. 4. The distributions of the maximum principal stress in a chain of brittle elastic beads in the reference simulation at different times.

Fig. 5a illustrates the largest value of the maximum principal stress in the various beads in the reference simulation. Here the grey line represents the first bead located closest to the impacting bar, at the right of the chain, while the black line represents the tenth bead located at the left end of the chain. Time is normalised by  $t_{sp}$ , the impact bar/bead separation time  $t_{sp} = 2L_s/c_s = 80 \mu s$ , the time needed for the stress wave to travel a distance equivalent to twice the length of the impacting bar, where  $L_s$  is the length of the impacting bar and  $c_s$  is the wave speed in steel.

It is clear from Fig. 5a that the second elastic bead is the first to reach the tensile strength of glass (33 MPa) and thus is the first expected to fail in chain of brittle glass beads. We believe the very high maximum principal stress in the second glass bead is mainly due to the tensile stress generated as reflected stress at the free surface of the glass bead. On the other hand, the tensile stress reflected at the free surface of the first glass bead was mostly cancelled by the incoming compressive stress induced by the impactor. In addition, it shows that at the beginning of the simulation, the magnitude of the maximum principal stress in the first bead is much lower than that in the other spheres, except for the left three. Moreover, even if some particles reach the failure criteria in the left three spheres, it is only a local phenomenon that does not form the critical failure circle as shown in Fig. 4c. Also note that if the bead material has a tensile stress  $R_g$  below 25.6 MPa, then the first bead would be expected to fail first. Otherwise, the second bead is always the first damaged sphere in the chain. We then define a ‘transition failure stress’  $\sigma_t$ , which determines whether the first or the second bead would fail first under the given loading conditions. In this simulation,  $\sigma_t = 25.6$  MPa.

### 3.2. Effect of impact velocity

Fig. 6 shows the distributions of the maximum principal stresses along the chain under different impact velocities at time of 210  $\mu s$  after impact. When the impact velocity is 1.5 m/s, due to the low

impact velocity, the magnitude of the maximum principal stress in the beads is small. As a consequence, we can only find the critical failure circle in the second bead. No critical failure circles form in the other beads, as shown in Fig. 6a. Fig. 6c demonstrates the distribution of the maximum principal stress along the chain under the 5 m/s impact velocity. Similar to the reference simulation, the critical failure circle can form from the second closest bead first even though the first bead sustains the highest maximum principal stress near the impact location immediately after impact. In fact, even the left three beads can fail under such high impact velocity. Furthermore, the critical failure circle can also form in the first bead after a period of time. However, during the entire simulation, the maximum principal stress in the first bead is still much lower than that in the other spheres. Fig. 6d depicts the distribution of the maximum principal stress in the chain under the 10 m/s impact velocity. In this case, a few internal points fail. The other phenomena are similar to those in the 5 m/s impact velocity simulation. It has to be pointed out that although many new failure locations appear due to the higher magnitude of the stress wave, the final critical failure circle still appears at the second closest bead first, which is the same as in all other simulations.

When the impact velocity increases to 5 m/s or 10 m/s, it appears that the bottom of each brittle elastic bead can also be damaged due to the high magnitude of tensile stress generated by the high velocity impact at the beginning of the simulation. The failure points will appear at the same locations of the following brittle elastic beads, one by one, with the subsequent propagation of the stress wave.

Fig. 5b shows the largest value of the maximum principal stress in the various beads under the impact velocity of 10 m/s. Here, time is also normalised by  $t_{sp}$ . Similar to the reference simulation, the maximum principal stress of the first bead is much lower than that in the other spheres, except for the initial short simulation period. The corresponding transition failure stress is 245.6 MPa. Adopting a tensile strength of 33 MPa, some local points in the first bead will fail first under this impact velocity.

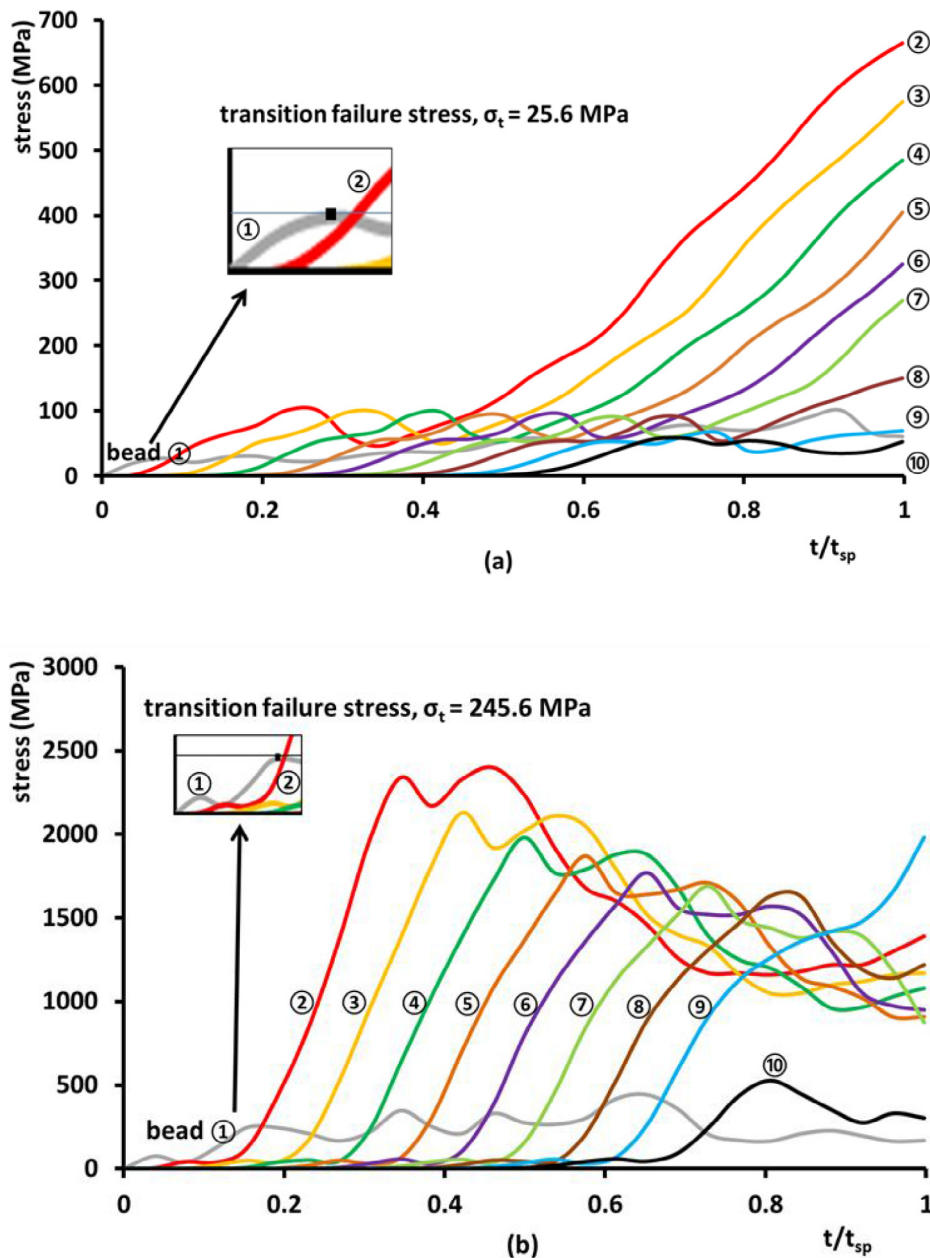


Fig. 5. Time history of the largest value of the maximum principal stress in the various beads in the chain under impact velocity of (a) 2.5 m/s; (b) 10 m/s.

As can be seen from the history of the largest maximum principal stress of the various beads shown in Fig. 5, immediately after the impact, the first bead will experience some relatively small tensile stresses first. Once the stress waves reach the second bead, much larger tensile stresses will be developed within it. As a result, whether the first or the second closest bead to the impacting bar will fail first depends on the maximum tensile stress level developed in the various beads and the strength of the material. If the tensile strength of the material is above this transition failure stress, then the second brittle elastic bead will fail first. Otherwise, it will be the first bead that experiences failure first. Fig. 7 shows the transition failure stress as a function of the impact velocity in the chain of brittle elastic beads. It clearly shows that the transition failure stress increases slowly when the impact velocity is small until it reaches 5 m/s. After that, the transition failure stress increases dramatically and almost linearly when the impact velocity is 12.5 m/s. Then the increasing

trend slows down when the impact velocity ranges from 12.5 m/s to 17.5 m/s. It will dramatically increase again as the impact velocity increases further.

To investigate whether the observed characteristics of this transition failure stress are universal, we show in Fig. 8 the non-dimensional failure stress for simulations with various material properties. Three groups of simulations are primarily presented. Real material properties of glass and steel ( $E_g = 70$  GPa,  $\rho_g = 2500$  kg/m<sup>3</sup>,  $E_s = 210$  GPa,  $\rho_s = 7800$  kg/m<sup>3</sup>) are used in the first group (Group 1). For the second group (Group 2), the Young's modulus of the beads and bars are quadrupled ( $4E_g = 280$  GPa,  $4E_s = 840$  GPa) while keeping other properties unchanged. Similarly, the density of the beads and bars are quadrupled ( $4\rho_g = 10000$  kg/m<sup>3</sup>,  $4\rho_s = 31200$  kg/m<sup>3</sup>) while keeping other properties unchanged in the third group (Group 3). Fig. 8 reports the non-dimensional analysis results, where the transition failure stress is normalised by the Young's modulus  $E$  of the

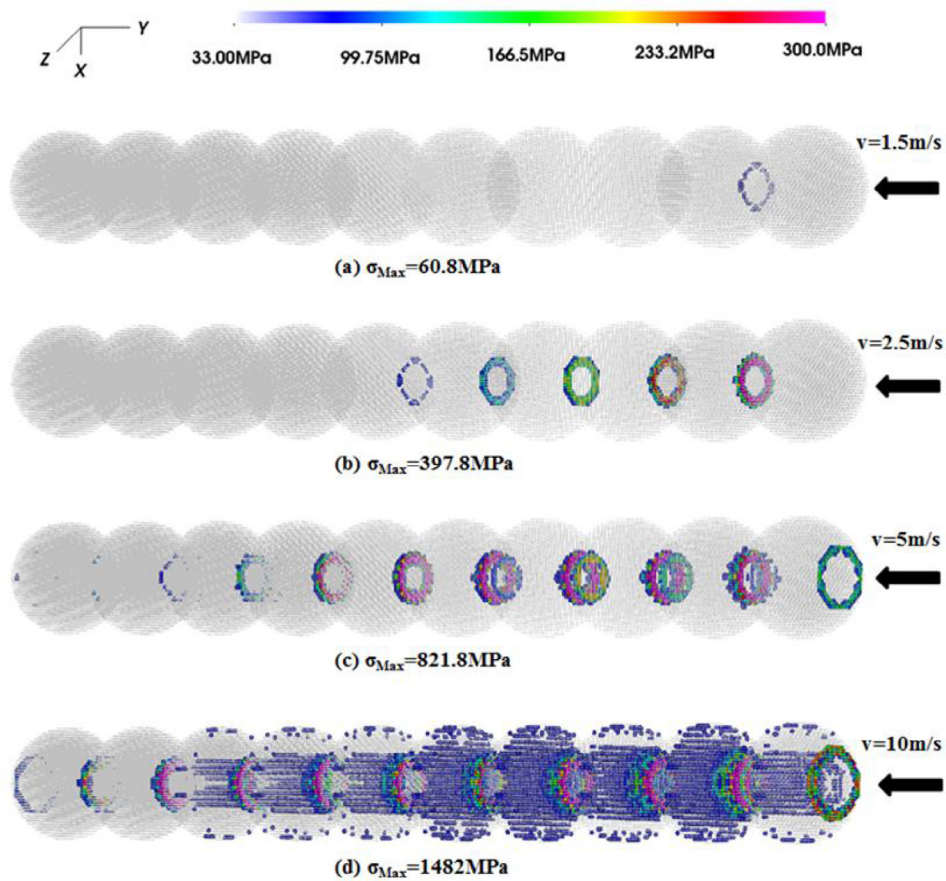


Fig. 6. The distribution of the maximum principal stress of a chain of spherical beads at time 210  $\mu$ s under impact velocity of (a) 1.5 m/s, (b) 2.5 m/s, (c) 5 m/s and (d) 10 m/s.

material under impact, while the impact velocity is normalised by the elastic wave velocity  $c$  of the material under impact. It shows that the simulation results of the three different groups well collapse into one curve, which indicates that the characteristics of this

transition failure stress will not change as long as the ratios of the Young's modulus and density of the impactor and the target are kept unchanged. The purple line in Fig. 8 represents the average results from these three groups.

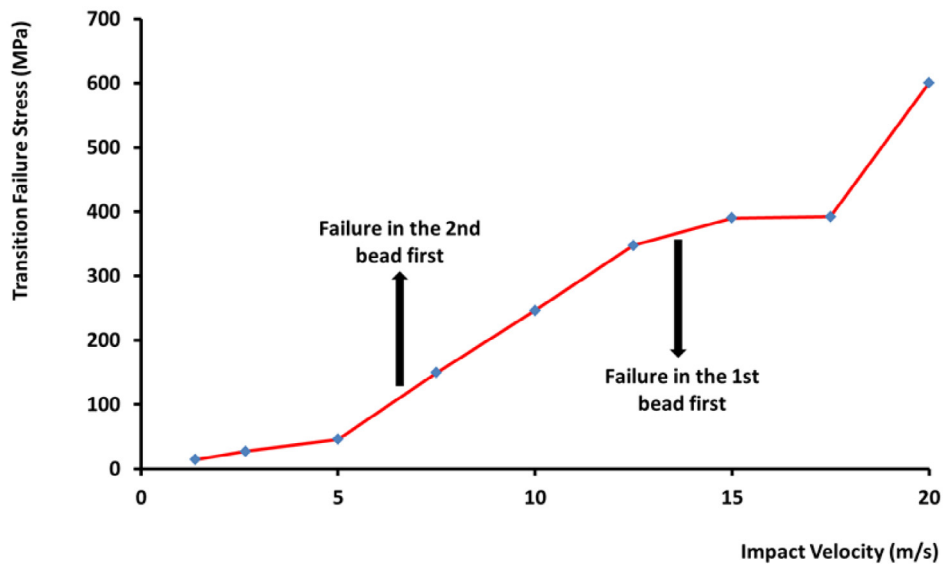


Fig. 7. Transition failure stress vs. impact velocity.

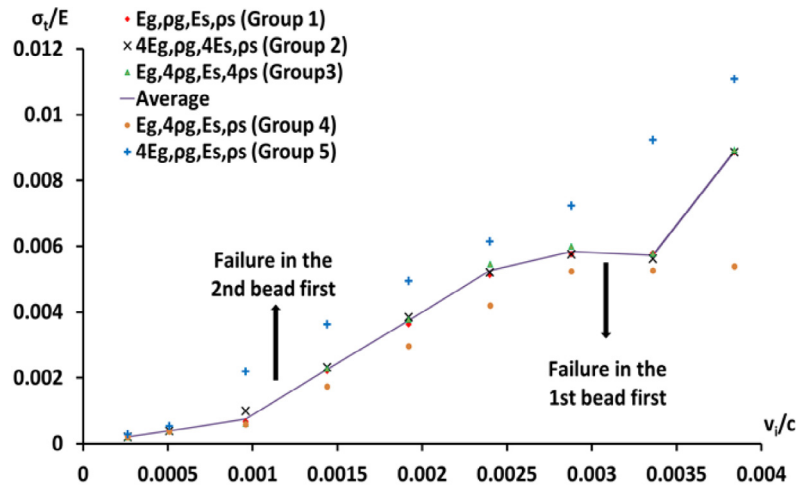


Fig. 8. Non-dimensional transition failure stress vs. non-dimensional impact velocity.

Additionally, two more groups of simulations with only a single change made to either the Young's modulus or the density of the beads are shown in Fig. 8. For the case where only the density changes (Group 4), the normalised transition failure stress is close to the average line of the previous three groups of simulations, especially when the normalised impact velocity is small. However, if we only change the Young's modulus of the granular chain (Group 5), the normalised transition failure stresses are well above the average values from Groups 1–3, as also shown in Fig. 8. This further suggests that the characteristics of the transition failure stress are dependent on the ratios of the Young's modulus and density of both the impactor and the target.

### 3.3. Effect of the length of impacting bar

Numerical simulations are carried out to investigate the effect of impulse duration on the dynamic responses of the brittle elastic beads by varying the length of the impacting bar between 100 mm and 400 mm, as outlined in the third row of Table 1. Since the magnitude of the initial impulse is independent on the length of the impacting bar, the stress histories will be exactly the same in these four simulations until the unloading of the stress wave starts, i.e. after about 40  $\mu$ s in the 100 mm length impacting bar simulation. Indeed, under impact velocity of 2.5 m/s, the transition failure stress in all these four simulations is 25.6 MPa and is not affected by the change of the length of impacting bar. As can be foreseeable, if the length of the impacting bar continues to decrease, due to the reduction of the loading duration, the transition failure stress may change.

The distributions of the maximum principal stress of brittle elastic beads chain impacted by the right bar of different lengths with impact velocity of 2.5 m/s at time of 250  $\mu$ s are shown in Fig. 9. Despite the similar stress distributions at the starting stage, the magnitudes of the maximum principal stress are obviously different in these four simulations at the later stages, such as at time 250  $\mu$ s. As can be seen in Fig. 9a, the critical failure circle can only form from the second to the fourth brittle elastic spheres when the length of the impacting bar is 100 mm. When the impacting bar is 300 mm long, the critical failure circle can also be found in the eighth bead as shown in Fig. 9c. Furthermore, as can be seen in Fig. 9c, after a long period of time, some points near the impact location of the first bead also fail when the impacting bar is 300 mm. When the impacting bar increases to 400 mm long, similar phenomenon can be found as shown in Fig. 9d.

### 3.4. Comparison simulations – experiments

The previous simulations indicate that there exists a transition for a given material from the fracture of the second closest bead to the impactor to the fracture of the first one as impact velocity is increased. This is indeed what was observed experimentally (Fig. 1), although the experimental transition velocity does not quantitatively match the numerical one. The reason of this discrepancy is mainly due to the fact that the numerical study focused only on the first fracture point in the bead (i.e. the first material point reaching the material fracture strength). Experimentally, this first fracture instant cannot be easily detected and only considerably damaged beads will be evidenced, which can therefore increase the apparent transition velocity measured in the experiment. Moreover, there is probabilistic variability in the material properties of the beads used in experiment, leading to a more scattered transition, such as small variability in the Weibullian strength of the various glass beads. For example, the real fracture strength of the individual glass beads can be different from the single value of 33 MPa used in the simulation. Hence, more comprehensive experiments are needed for closer comparisons with the simulations, which may lead to refining the numerical model.

## 4. Conclusions

In this study, a three dimensional simulation of a chain of 10 brittle elastic beads under impact loading is performed using the Material Point Method. The simulation results show that after some time, the magnitude of the maximum principal stress in the closest bead to the impacting bar may be lower than that in the second and the rest of the beads. As a result, whether the first or second brittle elastic bead fails first is dependent on the maximum tensile stress level developed in the various beads and the tensile strength of the material. The notion of 'transition failure stress' is thus defined in this study. If the fracture strength of the material is above this transition failure stress, then the second bead will fail first. Otherwise, it is the first bead that will fail first. Non-dimensional analysis of the proposed transition failure stress indicates that the experimentally observed failure evolution process is universal as long as the ratios of the Young's modulus and density of the impactor and the target are kept unchanged. The existence of a transition failure stress in a chain of brittle elastic glass beads, as well as the important effect of the velocity and length of the impacting bar on the

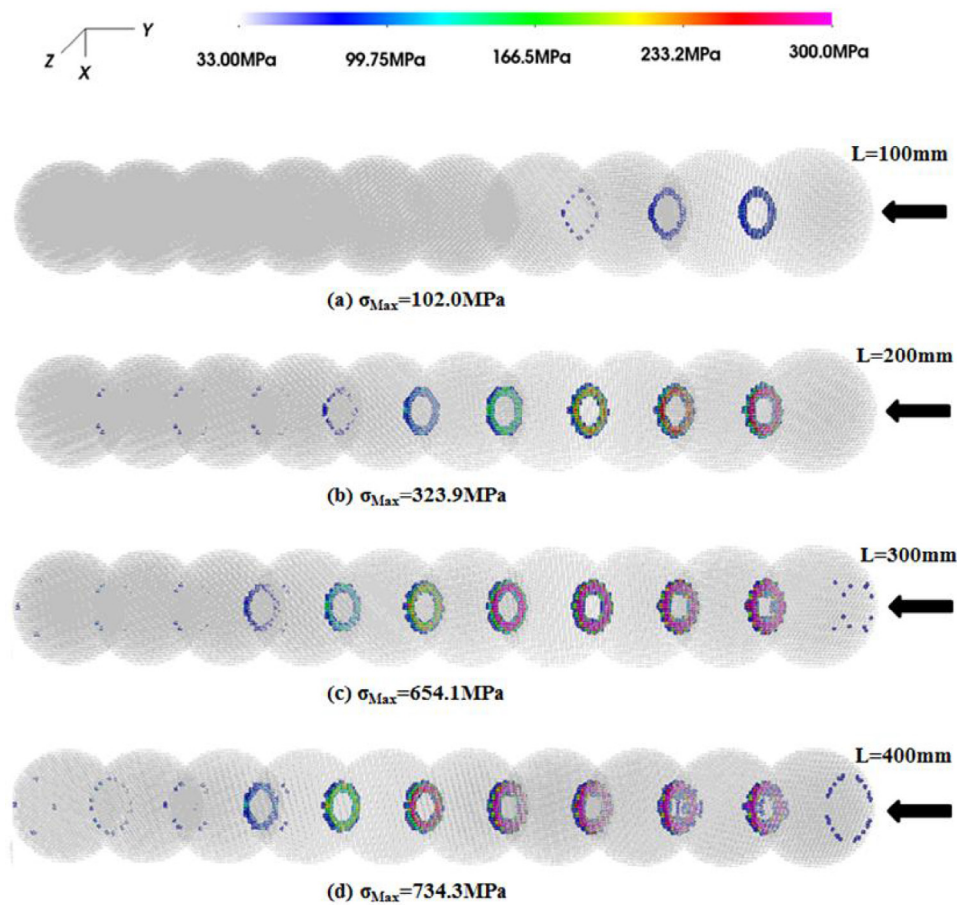


**Fig. 9.** The distributions of the maximum principal stress in the beads chain under the impact of bars with different length, under an impact velocity of 2.5 m/s and at time 250  $\mu$ s.

critical failure circle, provide an important framework for the study of more realistic situations, e.g. sand protection of building against impact or bulletproof vests.

### Acknowledgements

The work was supported in part by the Australian Research Council through Discovery Projects (DP130101291 and DP140100945), by the Faculty of Engineering & Information Technologies at The University of Sydney through the Faculty Research Cluster Program, and by the National Natural Science Foundation of China through Grant No. 11232003.

### References

- [1] Santamarina J, Klein K, Fam M. Soils and waves. New York: John Wiley; 2001.
- [2] Walton OR, Braun RL. Viscosity, granular-temperature, and stress calculations for shearing assemblies of inelastic, frictional disks. *J Rheol* 1986;30:949–80.
- [3] Pak R, Guzina B. Three-dimensional wave propagation analysis of a smoothly heterogeneous solid. *J Mech Phys Solids* 1995;43:533–51.
- [4] Pal RK, Awasthi AP, Geubelle PH. Characterization of wave propagation in elastic and elastoplastic granular chains. *Phys Rev E* 2014;89:012204.
- [5] Parab ND, Claus B, Hudspeth MC, Black JT, Mondal A, Sun J, et al. Experimental assessment of fracture of individual sand particles at different loading rates. *Int J Impact Eng* 2014;68:8–14.
- [6] Shi C, Wang M, Zhang K, Cheng Y, Zhang X. Semi-analytical model for rigid and erosive long rods penetration into sand with consideration of compressibility. *Int J Impact Eng* 2015;83:1–10.
- [7] Curran D, Seaman L, Cooper T, Shockey D. Micromechanical model for comminution and granular flow of brittle material under high strain rate application to penetration of ceramic targets. *Int J Impact Eng* 1993;13:53–83.
- [8] Huang J, Xu S, Hu S. Influence of particle breakage on the dynamic compression responses of brittle granular materials. *Mech Mater* 2014;68:15–28.
- [9] Omidvar M, Malioche JD, Bless S, Iskander M. Phenomenology of rapid projectile penetration into granular soils. *Int J Impact Eng* 2015;85:146–60.
- [10] Proud W, Chapman D, Williamson D, Tsembelis K, Addiss J, Bragov A, et al. The dynamic compaction of sand and related porous systems. *Shock compression of condensed matter* 2007;1403–8.
- [11] Badham H, Chalmers M, Nguyen T-T, Proud W. The propagation of blast pulses through dampened granular media. *Shock compression of condensed matter* 2015.
- [12] Wills BA. Wills' mineral processing technology: an introduction to the practical aspects of ore treatment and mineral recovery. Butterworth-Heinemann; 2011.
- [13] Brown ET. Block Caving Geomechanics: International Caving Study 1997–2004. Julius Kruttschnitt Mineral Research Centre, The University of Queensland, 2007.
- [14] Hiestand EN. Mechanical properties of compacts and particles that control tableting success. *J Pharm Sci* 1997;86:985–90.
- [15] Ben-Nun O, Einav I. The role of self-organization during confined comminution of granular materials. *Phil Trans R Soc A* 2010;368:231–47.
- [16] Valdes JR, Fernandes FL, Einav I. Periodic propagation of localized compaction in a brittle granular material. *Granul Matter* 2012;14:71–6.
- [17] Guillard F, Golshan P, Shen L, Valdes JR, Einav I. Dynamic patterns of compaction in brittle porous media. *Nat Phys* 2015;11:835–8.
- [18] Job S, Melo F, Sokolow A, Sen S. How Hertzian solitary waves interact with boundaries in a 1D granular medium. *Phys Rev Lett* 2005;94:178002.
- [19] Pal RK, Awasthi AP, Geubelle PH. Wave propagation in elasto-plastic granular systems. *Granul Matter* 2013;15:747–58.
- [20] Wang S, Nesterenko V. Attenuation of short strongly nonlinear stress pulses in dissipative granular chains. *Phys Rev E* 2015;91:062211.
- [21] Harlow FH. The particle-in-cell computing method for fluid dynamics. *Method Comput Phys* 1964;3:319–43.

- [22] Sulsky D, Chen Z, Schreyer HL. A particle method for history-dependent materials. *Comput Method Appl Mech Eng* 1994;118:179–96.
- [23] Chen Z, Hu W, Shen L, Xin X, Brannon R. An evaluation of the MPM for simulating dynamic failure with damage diffusion. *Eng Fract Mech* 2002;69:1873–90.
- [24] Bardenhagen S, Brackbill J, Sulsky D. The material-point method for granular materials. *Comput Method Appl Mech Eng* 2000;187:529–41.
- [25] Sulsky D, Schreyer HL. Axisymmetric form of the material point method with applications to upsetting and Taylor impact problems. *Comput Method Appl Mech Eng* 1996;139:409–29.
- [26] Bardenhagen S, Guilkey JE, Roessig K, Brackbill J, Witzel W, Foster J. An improved contact algorithm for the material point method and application to stress propagation in granular material. *CMES-Comput Model Eng Sci* 2001;2:509–22.
- [27] Guilkey J, Harman T, Luitjens J, Schmidt J, Thornock J, de St Germain J, et al. Uintah user guide, in: SCI Institute Technical Report, 2009. <http://uintah-build.sci.utah.edu/trac/wiki/Documentation>.
- [28] Childs H, Brugger E, Whitlock B, Meredith J, Ahern S, Pugmire D, et al. Vist: An End-User Tool For Visualizing and Analyzing Very Large Data, in: *High Performance Visualization-Enabling Extreme-Scale Scientific Insight*, 2012.